

## Article

# The Effect of Thin Film Fabrication Techniques on the Performance of rGO Based NO<sub>2</sub> Gas Sensors at Room Temperature

Shazrah Shahzad <sup>1,†</sup> , Huaipeng Wang <sup>1,†</sup>, Weiwei Li <sup>1,\*</sup>, Yilin Sun <sup>2</sup>, Dan Xie <sup>1,\*</sup> and Tianling Ren <sup>1</sup>

- <sup>1</sup> School of Integrated Circuits, Tsinghua University, Beijing 100084, China; luoss18@mails.tsinghua.edu.cn (S.S.); whp20@mails.tsinghua.edu.cn (H.W.); rentl@tsinghua.edu.cn (T.R.)
- <sup>2</sup> School of Integrated Circuits and Electronics, Beijing Institute of Technology, Beijing 100081, China; sunyl@bit.edu.cn
- \* Correspondence: kgdliweiwei@163.com (W.L.); xiedan@tsinghua.edu.cn (D.X.)
- † These authors contributed equally to this work.

**Abstract:** Reduced graphene oxide (rGO) has attracted enormous interest as a promising candidate material for gas detection due to its large specific surface areas. In our work, rGO films were fabricated on a large scale using dip-coating and spin-coating methods for the detection of nitrogen dioxide (NO<sub>2</sub>) gas at room temperature. The influence of different test environments on the sensing performance, including the test atmosphere, gas flow and gas pressure was evaluated. The response time of the dip-coating method was 573 s with a long recovery period of 639 s and for the spin-coating method, the response time and recovery time was 386 s and 577 s, respectively. In addition, the spin-coated sensor exhibited high selectivity to NO<sub>2</sub>, with the response increasing by more than 20% (for 15 ppm NO<sub>2</sub>) as compared with that for HCHO, NH<sub>3</sub>, and CH<sub>4</sub>. Our results indicated that the spin coating method was more suitable for rGO-based gas sensors with higher performance.

**Keywords:** reduced graphene oxide; fabrication methods; NO<sub>2</sub> gas sensor; room temperature



**Citation:** Shahzad, S.; Wang, H.; Li, W.; Sun, Y.; Xie, D.; Ren, T. The Effect of Thin Film Fabrication Techniques on the Performance of rGO Based NO<sub>2</sub> Gas Sensors at Room Temperature. *Chemosensors* **2022**, *10*, 119. <https://doi.org/10.3390/chemosensors10030119>

Academic Editor: Manuel Aleixandre

Received: 10 February 2022

Accepted: 16 March 2022

Published: 21 March 2022

**Publisher's Note:** MDPI stays neutral with regard to jurisdictional claims in published maps and institutional affiliations.



**Copyright:** © 2022 by the authors. Licensee MDPI, Basel, Switzerland. This article is an open access article distributed under the terms and conditions of the Creative Commons Attribution (CC BY) license (<https://creativecommons.org/licenses/by/4.0/>).

## 1. Introduction

In recent years, the detection of toxic gases has attracted great attention owing to the harmful effects these gases have on health [1,2]. Poisonous gases, including nitrogen dioxide (NO<sub>2</sub>), formaldehyde (HCHO) and sulfur dioxide (SO<sub>2</sub>) are prone to not only causing respiratory diseases and neurological disorders, but are also responsible for air pollution and are detrimental to the environment [3–5].

NO<sub>2</sub>, is considered one of the most harmful gases to human health and the environment. It is formed as a result of multiple sources in both daily life and chemical industry, such as vehicle exhaust and fossil fuel combustion [6]. Low concentrations of NO<sub>2</sub>, at levels greater than 1 ppm, can cause serious damage to the human respiration system and lung tissue, and increase the risk of emphysema and bronchitis. Furthermore, NO<sub>2</sub> is not only a component of acid rain, but also participates in ozone formation, which may lead to the formation of micro-particles in the air [7,8]. In these regards, the detection of harmful NO<sub>2</sub> gas has emerged as one of the most important aspects of sensing techniques and research.

Reduced graphene oxide (rGO) is regarded as a renowned derivative of graphene, due to its ease of production, especially via low-cost solution methods. Moreover, it demonstrates unique controllable abilities, and enhances the capabilities of other sensing elements [9]. These unique properties then allow the use of rGO as a promising electrode (sensing) material in various applications, e.g., in flexible/wearable supercapacitors [10,11], sensing [12,13], microwave absorbers [14], photocatalytic decontamination [15], and as electrodes in lithium-ion and sodium-ion batteries [16,17]. For gas sensing applications, carbon-based nanomaterials including rGO offer certain advantages, such as improved

carrier mobility and brilliant contact with nanometer-sized sensing materials [18], owing to the presence of multiple active adsorption regions with a large surface area.

Recently, rGO-based NO<sub>2</sub> sensors have been widely studied due to their excellent performances. Cui et al. rendered sensors extremely sensitive to NO<sub>2</sub> by applying a transient voltage across rGO to produce defects such as pits, epoxide and other functional groups such as GO [19]. Shi et al. synthesized a chemically modified rGO bearing sulfur functional group decoration, which showed high sensitivity, selectivity, reversibility, and 16.4 times stronger responses compared with conventional rGO-based sensors [20]. Zhou et al. used MoS<sub>2</sub>, a type of transition metal chalcogenides (TMDs), to fabricate rGO/MoS<sub>2</sub> hybrids for use in ultrahigh sensitivity to NO<sub>2</sub> applications, with the detection limit down to 5.7 ppb. The improved sensitivity was attributed to both rGO and MoS<sub>2</sub> serving as sensitive layers [21]. Pristine rGO, doped rGO, functionalization of rGO and rGO-based composites were used to study the mechanism and performances of their NO<sub>2</sub> detection devices [6]. Hung et al. synthesized the nanocomposites of rGO and WO<sub>3</sub> nanowires hydrothermally, and the subsequent rGO/WO<sub>3</sub> nanocomposite sensors showed excellent sensing performance with a theoretical detection limit of 138 ppb [22]. Kuchi et al. synthesized GO using electrochemical exfoliation, obtained TiO<sub>2</sub>-rGO composite nanofibers via hydrothermal method, and demonstrated that the sensors exhibited a high sensitivity of 7.1 to 2.75 ppm of NO gas [23]. Qian et al. revealed a novel high-efficiency electrocatalyst composed of hierarchical sea urchin-like Prussian blue@palladium core-shell heterostructures supported on nitrogen-doped rGO using a combined hydrothermal assembly and freeze-drying process, which exhibited a wide detection range and low detection limit for guanine assays [24,25].

However, despite the existing research in material design, large-scale fabrication still remains a key issue suppressing development of the industrial production of rGO-based NO<sub>2</sub> gas sensors. Traditional precise fabrication methods used in laboratory settings are complicated and expensive, hence, not suitable for large-scale fabrication. Dip coating and spin coating are two simple fabrication methods that can be easily operated, and have already been used for large-area production [26,27]. In our research work, rGO-based gas sensors were prepared through dip coating and spin coating methods, respectively, and their different gas-sensing performances were investigated at room temperature. The motivation for the study is to analyze the method best suited for producing rGO-based NO<sub>2</sub> sensors and to evaluate sensitivity and stability in the sensing properties to low concentrations of target gases at room temperature, which can be further used in the preparation of sensors based on other different carbon materials. This provides guidance to the design of gas sensors with enhanced performances.

## 2. Materials and Methods

The experimental section is divided into three sections, i.e., characterization of rGO, sensor fabrication and gas sensing measurement set-up. The rGO dispersion is produced by chemically reducing graphene oxide (GO) (500–1000 m<sup>2</sup> g<sup>-1</sup>, 2 mg mL<sup>-1</sup>, sheet diameter > 500 nm solution) using an optimized method from Li et al. [28].

### 2.1. Characterization of rGO

For the obtained rGO, scanning electron microscopy (SEM) measurements were performed at NOVA NANO SEM 450 FEL, transmission electron microscope (TEM) images were conducted using JEM-2100F at 80 kV. Raman spectra were collected on a LabRAM HR Evolution spectrometer (HORIBA Jobin Yvon, Paris, France) with a 532 nm excitation laser source. X-ray diffraction (XRD) patterns were acquired on a D8-Advanced X-ray diffractometer (Bruker, Ettlingen, Germany) using Cu K $\alpha$  radiation ( $\lambda = 1.5418 \text{ \AA}$ ). X-ray photoelectrospectrometer (XPS) (PHI-5300, PHI, Waltham, MA, USA) was used to study defect levels of rGO.

## 2.2. Sensor Fabrication

Sensor devices are fabricated by conventional photolithography and lift-off techniques on silicon substrate capped with 300 nm thick SiO<sub>2</sub>. The electron beam evaporation of Ti/Au (10 nm/50 nm) was performed to form the interdigitated electrodes on the Si/SiO<sub>2</sub> substrate. The finger width and gap width of electrodes were both 10 μm.

### 2.2.1. Dip Coating

In this section, the rGO thin film gas sensor is prepared by dip coating. The specific experimental process is shown in Figure 1a as follows:

1. Pre-cleaned titanium/gold (Ti/Au) interdigitated electrode based on Si/SiO<sub>2</sub> substrate is vertically immersed in a beaker filled with chemically reduced rGO aqueous dispersion (0.25 mg mL<sup>-1</sup>).
2. The electrode is taken out after an immersion for 20 s.
3. Small amount of solution attaches to the electrode surface which needs to be removed via heat treatment. Hence, the electrode is air-dried (12 h) under normal temperature and pressure to remove the solvent and to obtain a dried rGO sensitive film.

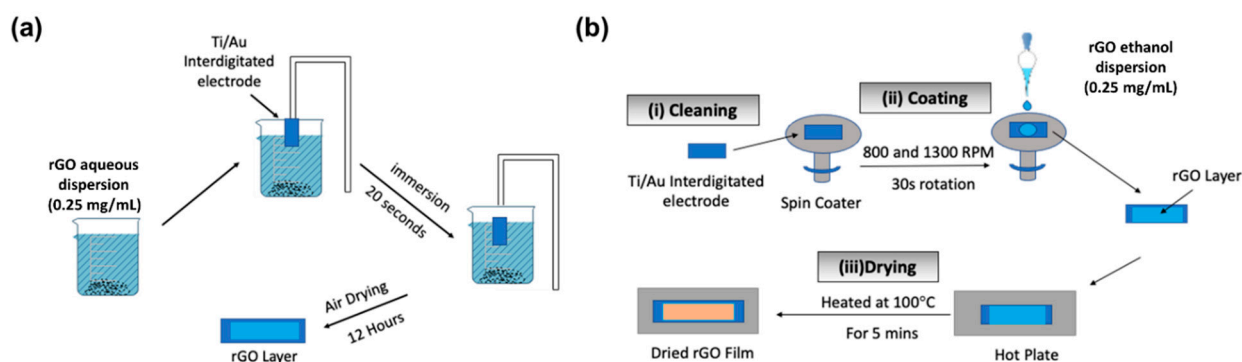


**Figure 1.** Schematic illustration of (a) the dip coating, and (b) the spin coating method for sensing layer deposition.

### 2.2.2. Spin Coating

In this section, the rGO sensor film is prepared by spin coating method, the specific experimental process as shown in Figure 1b, is as follows:

1. Pre-cleaned Ti/Au interdigitated electrode based on Si/SiO<sub>2</sub> substrate is fixed on the spin coater, and a small volume of chemically reduced rGO dispersion in ethanol (0.25 mg/mL) is dropped on the interdigitated electrode surface via micropipette, and the electrode surface is fully covered by the rGO dispersion for 60 s;
2. The spin coater is then rotated at 800 r/min and 1300 r/min while, with rotation time as 30 s.
3. Post rotation. The rGO dispersion is spread evenly on the surface of the interdigitated electrode to form rGO film.

In order to promote solvent volatilization, the coated electrode is placed on a hot plate at 100 °C for 5 min to obtain the dried rGO film.

## 2.3. Gas Sensing Measurement

The sensors are fabricated on the interdigitated electrodes, and are connected with conductive silver paste for gas testing. The measurements are recorded in real time using Keithley 2700 which measures the sensor resistance in the gas measurement system at room temperature (~23 °C). The equilibrium gas is dry air which provides an inert environment and also dilutes the concentration of target gas. This is modulated to achieve the required gas concentration by use of a mass flow controller, as shown in Figure 2. The gas-sensing property or sensor response can be defined as change in percentage resistance  $S$  (%) by the

following formula:  $S(\%) = (R_a - R_g)/R_a \times 100\%$ . In this equation, initial resistance in inert atmosphere (dry air) is  $R_a$  and the observed resistance in target gas ( $\text{NO}_2$ ) is defined as  $R_g$ .

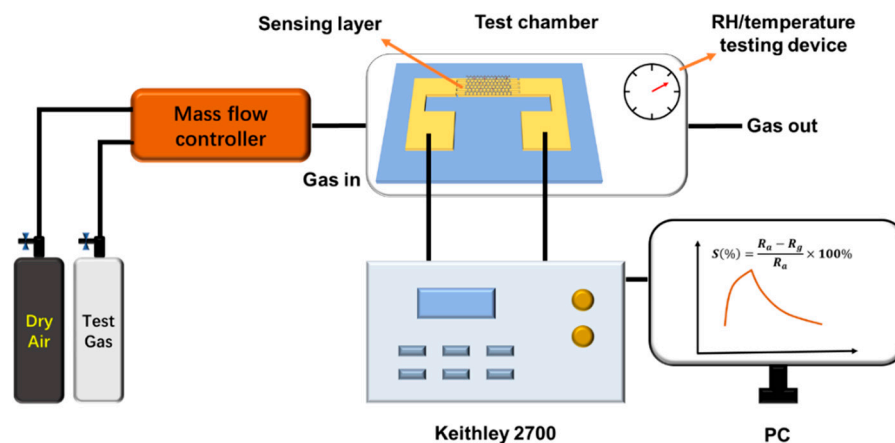


**Figure 2.** Diagram of the gas-sensing testing system.

During the test, the sensor showed sensitivity to  $\text{NO}_2$  gas. For practical application environment, all experiments are carried out with dry air as carrier gas. The purpose of these is to ascertain which of these two techniques can be employed and developed for future use as an industrial route for production of  $\text{NO}_2$  gas sensor. The sensor testing will yield a feasible industrial route at the end of experimental testing which we will then recommend.

### 3. Results and Discussion

#### 3.1. Characterization of High-Quality rGO Solutions

To ensure the high performance of gas sensor, it is necessary to produce rGO solutions with high quality. By using the method reported by Li et al. [28], we further optimized the post-treatment to make rGO solutions as uniform as possible. A tank ultrasonic process was performed using KH5200B ultrasonic bath from Hechuang ultrasonic instrument Co., Ltd. (Jiangsu, China. 200 W, 50 Hz). As shown in Figure 3a, after adjusting the appropriate ultrasonic time to 10 min, rGO solution was observed to be ultra-uniform and there was no stratification even after high-speed centrifugation at speed of  $12,000 \text{ r min}^{-1}$ .

The morphology and structure properties of the synthesized rGO were then characterized by TEM, SEM, Raman spectra, XPS and XRD (Figure 3b–f). TEM and SEM images revealed the size and morphology of dispersed rGO nanosheets. The wrinkled surface of rGO was revealed by TEM (Figure 3b), the formation of which was in response to the reduction process [29], which was useful for gas sensing and better recovery during gas sensing [30]. Most of the rGO nanosheets were complete and their size reached up to several tens nanometers, with some even at the millimeter-level (Figure 3c).

Raman spectra were performed to investigate the defects of rGO in a non-destructive way, as shown in Figure 3d, rGO sheets presented typical D band and G band, which correspond to disordered and graphitic regions, respectively. The  $I_D/I_G$  ratio is 1.02, indicating the defects appearing after the reduction process and successful removal of oxygen functional groups [31]. To evaluate the defect level of rGO, XPS was carried out and only few function groups of C-O and C=O were found, indicating the defects were fully suppressed (Figure 3e).

XRD was used to characterize the as-prepared rGO. As shown in Figure 3f, rGO showed a broad peak at  $2\theta$  of about  $20.5^\circ$ , which indicated the (002) lattice plane of the  $\text{sp}^2$  hybridized carbon hexagonal structure [32].

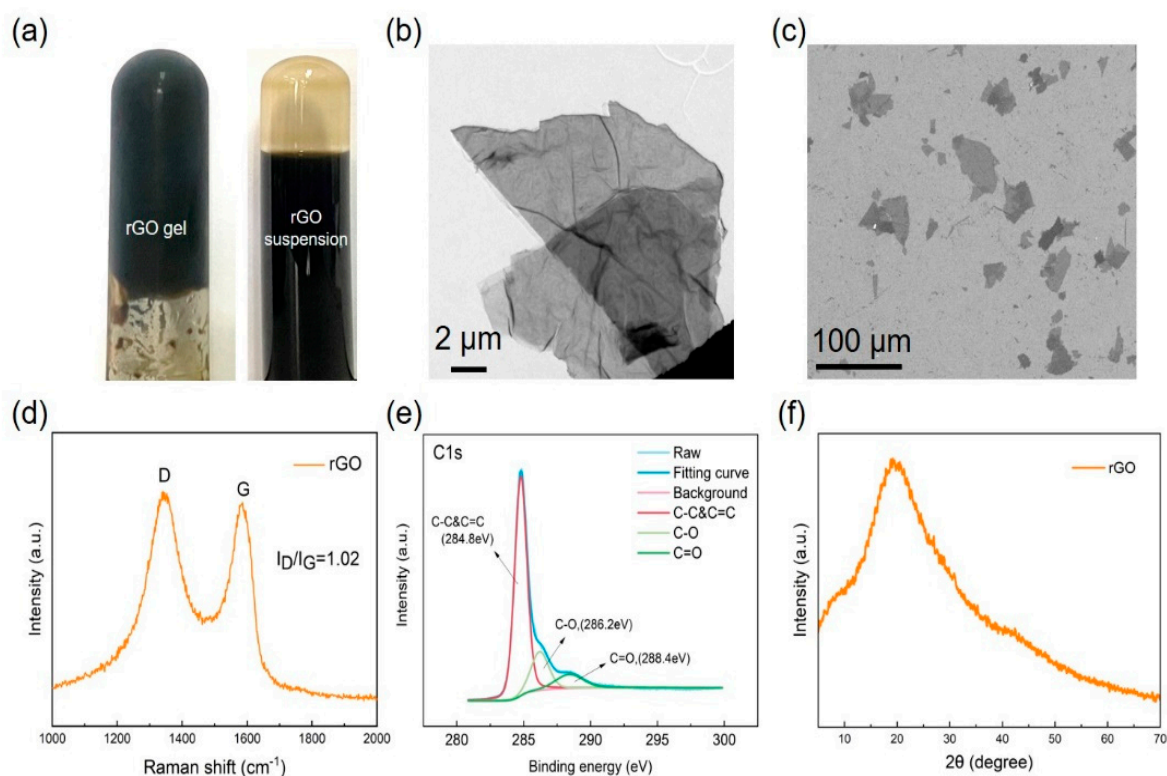


**Figure 3.** Basic characterizations of rGO. (a) Picture of the freshly obtained rGO. Left: rGO gel, right: rGO suspension after  $12,000 \text{ r min}^{-1}$ . (b) TEM, (c) SEM of rGO from different magnifications. (d) Raman spectra of rGO. (e) C 1s XPS spectra of as-prepared rGO. (f) XRD patterns of rGO.

### 3.2. Gas Sensing Mechanism of rGO

The gas sensing mechanism of rGO is credited to the direct charge transfer between sensing materials and the target gas and when absorption occurs on the sensing layer. Whilst rGO showcases a typical p-type semiconductor behavior [33],  $\text{NO}_2$ , an oxidizing gas, behaves as an electron acceptor [34]. When target gas is adsorbed on the p-type semiconductor it results in an increase in hole concentration which decreases the resistance vis-a-vis increases the electrical conductivity as can be observed in Figures 4 and 5. The increase in conductivity is measured using Keithley 2700 and is directly proportional to the concentration of target gas. The reduced graphene oxide is used as it is known to accelerate the electron-transfer process, which influences the sensing process resulting in a prominent change in the electrical characteristics.

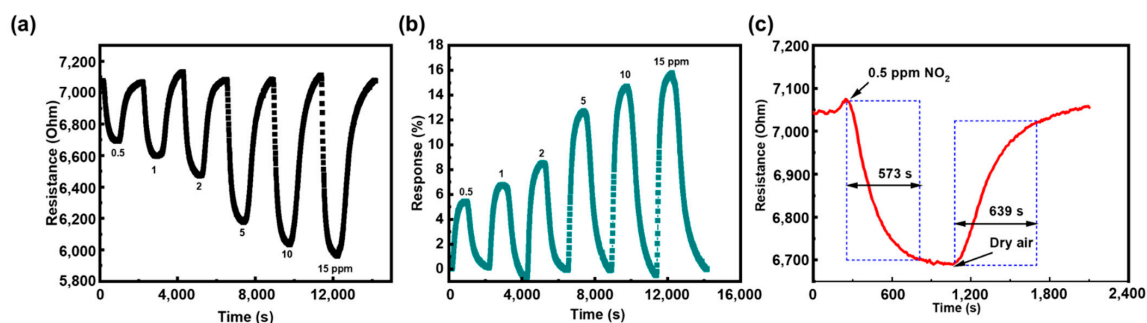


**Figure 4.** Response of rGO film (dip coating) in 0.5–15 ppm  $\text{NO}_2$ . (a) Real-time sensing response curve, (b) Real-time resistance change curve of rGO film prepared by dip coating from 0.5–15 ppm  $\text{NO}_2$  with dry air (c) Real-time resistance change curve of rGO film prepared by dip coating in 0.5 ppm  $\text{NO}_2$  with dry air.

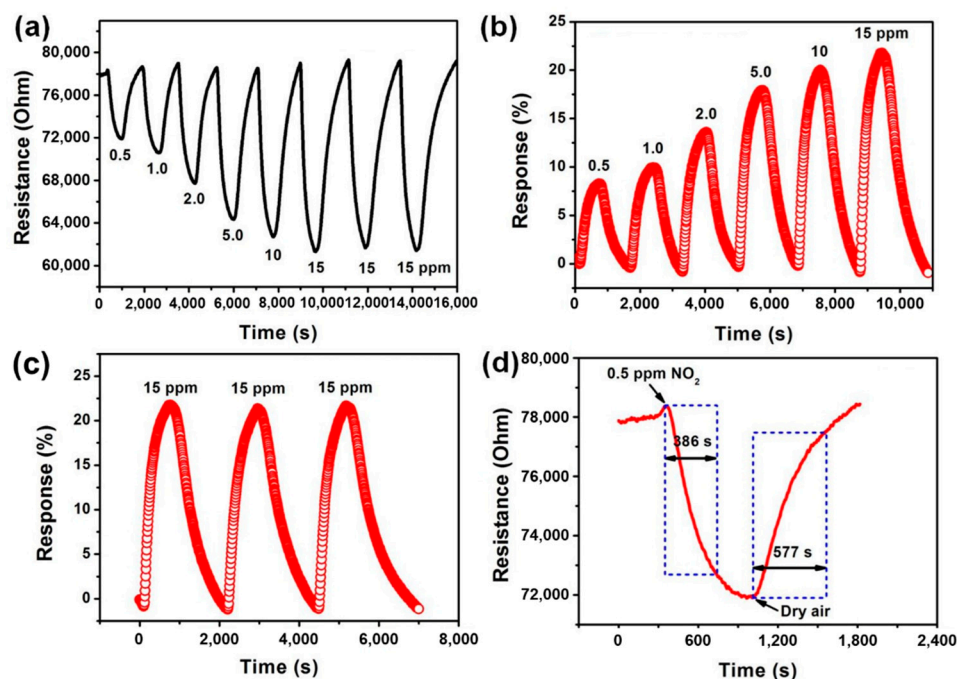


**Figure 5.** Response of rGO film (spin coating) from 0.5–15 ppm NO<sub>2</sub> (a) Real-time sensing resistance curve, (b) Real-time sensing response curve from 0.5–15 ppm, indicating response of 8.3%, 10.1%, 13.6%, 17.9%, 21.8% and 22.5%, respectively, (c) Reproducibility curve of rGO film prepared by spin-coated method, (d) Real-time resistance change curve of rGO film prepared by spin coating in 0.5 ppm NO<sub>2</sub>.

### 3.3. Gas Sensing Performances of Dip-Coated and Spin-Coated Sensors

#### 3.3.1. Gas Sensing Performance of Dip-Coated Sensor

A comparison of the sensing performance of rGO film produced by dip- and spin-coating techniques, was performed. When carrier gas was introduced, the resistance of the device could recover slowly. Figure 4a shows the resistance curve of rGO thin film prepared by dip coating in 0.5–15 ppm NO<sub>2</sub>. The real-time resistance change curve of rGO film prepared by dip coating from 0.5–15 ppm NO<sub>2</sub> with dry air can be observed in Figure 4b indicating a response of 5.4%, 6.7%, 8.4%, 12.7%, 14.6% and 15.7%, respectively. In Figure 4c, we can observe that the response time of the sensor to 0.5 ppm NO<sub>2</sub> is 573 s, while the recovery process is as long as 639 s.

The instability that was observed in the early stage of the test can be attributed to the simple operation of the dip coating method, where weak adhesion existed between the dispersion and the substrate, leading to the formation of the thin film with random coverage, thus the stability of the preparation plan needs to be improved. Therefore, it is difficult to form a uniform, stable performance and high quality rGO film on the surface of the interdigitated electrode. This was observed in gas sensing in the form of volatility and slow recovery performances which would suppress its future application as a gas sensor.

#### 3.3.2. Gas Sensing Performance of Spin-Coated Sensor

The real-time resistance/response curve is shown in Figure 5. The sensor showed sensitivity and gave a stable response to various concentrations of NO<sub>2</sub>. With the increase of NO<sub>2</sub> concentration, the sensor showed a significant increase in response. The results exhibit the sensor's responses to 0.5 to 15 ppm of NO<sub>2</sub> gas. The sensor was regulated by retesting the 15 ppm of target gas, this could be observed in Figure 5c, and showed the repeatability of the sensor. We can observe that the response of the sensor remained constant (~22%) for a set concentration of gas i.e., at 15 ppm for three consecutive cycles.

This was a positive aspect of the sensor, as it showed evidence for repeatability of the sensor device.

In Figure 5d, we can observe the real-time resistance curve of rGO film in 0.5 ppm  $\text{NO}_2$ . The response/recovery time was 386 s and 577 s, respectively, showing the complete response/recovery ability. On the basis of these data points we can claim that the spin-coating preparation of rGO film for gas sensing showed reversible characteristics, and achieved response/recovery ability under normal temperature conditions, indicating its potential application in real industry compared to the dip-coated rGO film at a low  $\text{NO}_2$  concentration.

Sensitivity and stability are considered key components of gas sensor research. The stability of the sensor based on spin-coating method was evaluated by testing the device over a period of seven days. The Figure 6a showed that the response of the sensor device remained constant to 15 ppm of target gas over a prolonged lifetime. For testing the sensor efficiency in real-time applications, a sensing test was required in humid conditions. As can be observed in Figure 6b, the sensor remained stable under humid conditions and showed an almost linear response. The linear response demonstrates proof that the spin-coated sensor can then be used in real world applications, due to its stability.

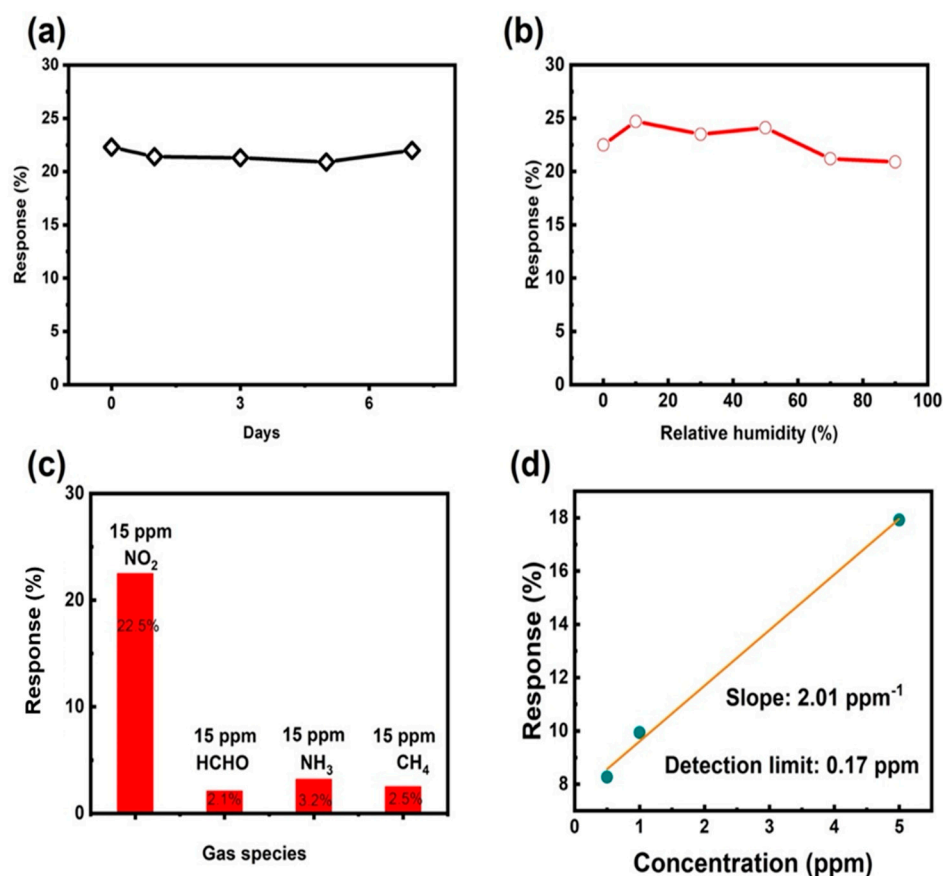


**Figure 6.** Stability, humidity, selectivity, and detection limit test of the rGO gas sensor prepared by spin coating. (a) Stability of gas sensor among one week. (b) Relative humidity–response curve. (c) Selectivity of gas sensor to different gases, including  $\text{NO}_2$ , HCHO,  $\text{NH}_3$  and  $\text{CH}_4$ . (d) Theoretical detection limit of the gas sensor responded to  $\text{NO}_2$ .

The selectivity of the gas sensor for the target gas is an aspect of gas sensor research, for this purpose the gas sensor as prepared by spin coating technique was then tested. The sensor was tested using  $\text{NO}_2$ , HCHO,  $\text{NH}_3$  and  $\text{CH}_4$  gases. The response shown by gas sensor for 15 ppm  $\text{NO}_2$  was remarkable at greater than 20% as compared to 2.1% for HCHO, 3.2% for  $\text{NH}_3$  and 2.5% for  $\text{CH}_4$  gas as shown in Figure 6c. Sensitivity is a key factor of

gas sensor research. It is determined by the slope of response (%) and gas concentration (ppm). Figure 6d shows the dependence of response on NO<sub>2</sub> concentration in the form of a linear relationship. To perform the method validation for the measurement of sensor response, the limit of detection (LOD) is calculated from the slope of the linear region of the response curve and the root-mean-square (RMS) deviation at the baseline. The LOD can be calculated as  $LOD = 3RMS/Slope$  [35]. The slope of response curve is calculated to be 2.01 ppm<sup>-1</sup>, and the detection limit of the gas sensor response to NO<sub>2</sub> is calculated to be 0.17 ppm.

To achieve a comprehensive understanding of the performance of the obtained rGO sensors, a comparison was introduced to summarize the recent typical works about NO<sub>2</sub> sensors based on different materials and their sensing performance (Table 1). Compared with other NO<sub>2</sub> sensors, the present rGO-based NO<sub>2</sub> gas sensor prepared by spin-coating showed more reliable sensitivity, faster response speed, reversible characteristics, lighter weight compared with metal/metal-oxide based devices, and can achieve response/recovery abilities under normal temperature conditions, proving the effectiveness of our spin-coating method.

**Table 1.** Gas sensing properties of sensors for detecting NO<sub>2</sub> gas (RT: Room temperature).

Materials	Operating Temperature (°C)	Detection Range (ppm)	Response Time (s)	Recover Time (s)	Ref.
Cu <sub>2</sub> O-rGO	RT	0.4–2	-	-	[36]
AuNP MWCNTs	RT	0.1–1	>600	-	[37]
SnO <sub>2</sub> nanowires	RT	>0.25	110	75	[38]
ZnO-rGO film	RT	100	566	547	[39]
Mo-doped SnS <sub>2</sub>	150	100	50.9	-	[40]
SnO <sub>2</sub> -ZnO	100	5–50	26.4	45	[41]
Phosphorene	RT	0.02–1	-	-	[42]
Pt@Cu <sub>3</sub> (HHTP) <sub>2</sub>	RT	0.1–3	780	-	[43]
rGO film	RT	0.5–15	386	577	This work

#### 4. Conclusions

The spin-coating fabrication route was implemented to rGO-based thin film sensors for NO<sub>2</sub> sensing, facilitating the formation of a coating film with higher uniformity and quality. Compared to the dip-coated sensor, the spin-coated sensor exhibited greater responses to a wide range of NO<sub>2</sub> concentrations (0.5–15 ppm) with a larger linear-response range. The repeatability and reversible characteristics of spin-coated sensors were demonstrated well, and the response/recovery time was measured as 386 s/577 s. The high stability of spin-coated sensors was revealed by monitoring the responses to 15 ppm NO<sub>2</sub> conditions over a long period of 7 days and under different humidity levels. Furthermore, the spin-coated sensor exhibited high selectivity to NO<sub>2</sub>, with the response increasing by more than 20% (for 15 ppm NO<sub>2</sub>) as compared with that for HCHO (2.1%), NH<sub>3</sub> (3.2%), and CH<sub>4</sub> (2.5%). In summary, we have successfully fabricated rGO film coated electrode arrays up to the size scale of inches using spin coating. This work provides a feasible strategy to fabricate rGO-based gas sensors by solution processable methods and exhibits great potential in developing large-scale commercial production and real-time gas detection through its advantages such as low cost, low toxicity and light weight of rGO.

**Author Contributions:** Conceptualization, S.S., H.W., W.L. and D.X.; data curation, S.S. and W.L.; formal analysis, W.L. and Y.S.; funding acquisition, Y.S. and D.X.; investigation, S.S., H.W. and W.L.; methodology, W.L.; supervision, D.X.; writing original draft, S.S.; writing review and editing, Y.S., H.W., D.X. and T.R. All authors have read and agreed to the published version of the manuscript.

**Funding:** This research was funded by the National Natural Science Foundation of China (Nos. 52072204 and 62104017), National Postdoctoral Program for Innovative Talents of China (BX20200049), and China Postdoctoral Science Foundation (2021M690013).

**Institutional Review Board Statement:** Not applicable.

**Informed Consent Statement:** Not applicable.

**Data Availability Statement:** Not applicable.

**Conflicts of Interest:** The authors declare no conflict of interest.

## References

1. Basu, S.; Bhattacharyya, P. Recent developments on graphene and graphene oxide based solid state gas sensors. *Sens. Actuators B Chem.* **2012**, *173*, 1–21. [[CrossRef](#)]
2. Niyat, F.Y.; Abadi, M.H.S. COMSOL-Based Modeling and Simulation of SnO<sub>2</sub>/rGO Gas Sensor for Detection of NO<sub>2</sub>. *Sci. Rep.* **2018**, *8*, 2149. [[CrossRef](#)] [[PubMed](#)]
3. Xiao, Y.; Yang, Q.; Wang, Z.; Zhang, R.; Gao, Y.; Sun, P.; Sun, Y.; Lu, G. Improvement of NO<sub>2</sub> gas sensing performance based on discoid tin oxide modified by reduced graphene oxide. *Sens. Actuators B Chem.* **2016**, *227*, 419–426. [[CrossRef](#)]
4. Liu, H.; Li, M.; Voznyy, O.; Hu, L.; Fu, Q.; Zhou, D.; Xia, Z.; Sargent, E.H.; Tang, J. Physically Flexible, Rapid-Response Gas Sensor Based on Colloidal Quantum Dot Solids. *Adv. Mater.* **2014**, *26*, 2718–2724. [[CrossRef](#)] [[PubMed](#)]
5. Li, X.; Wang, J.; Xie, D.; Xu, J.; Xia, Y.; Li, W.; Xiang, L.; Li, Z.; Xu, S.; Komarneni, S. Flexible room-temperature formaldehyde sensors based on rGO film and rGo/MoS<sub>2</sub> hybrid film. *Nanotechnology* **2017**, *28*, 325501. [[CrossRef](#)]
6. Lee, S.W.; Lee, W.; Hong, Y.; Lee, G.; Yoon, D.S. Recent advances in carbon material-based NO<sub>2</sub> gas sensors. *Sens. Actuators B Chem.* **2018**, *255*, 1788–1804. [[CrossRef](#)]
7. Andringa, A.-M.; Piliago, C.; Katsouras, I.; Blom, P.W.M.; de Leeuw, D.M. NO<sub>2</sub> Detection and Real-Time Sensing with Field-Effect Transistors. *Chem. Mater.* **2013**, *26*, 773–785. [[CrossRef](#)]
8. Huang, W.; Zhuang, X.; Melkonyan, F.S.; Wang, B.; Zeng, L.; Wang, G.; Han, S.; Bedzyk, M.J.; Yu, J.; Marks, T.J.; et al. UV-Ozone Interfacial Modification in Organic Transistors for High-Sensitivity NO<sub>2</sub> Detection. *Adv. Mater.* **2017**, *29*, 1701706. [[CrossRef](#)]
9. Li, D.; Müller, M.B.; Gilje, S.; Kaner, R.B.; Wallace, G.G. Processable aqueous dispersions of graphene nanosheets. *Nat. Nanotechnol.* **2008**, *3*, 101–105. [[CrossRef](#)]
10. Ghorbani, M.; Golobostanfard, M.R.; Abdizadeh, H. Flexible freestanding sandwich type ZnO/rGO/ZnO electrode for wearable supercapacitor. *Appl. Surf. Sci.* **2017**, *419*, 277–285. [[CrossRef](#)]
11. Shaikh, N.S.; Ubale, S.B.; Mane, V.J.; Shaikh, J.; Lokhande, V.; Praserthdam, S.; Lokhande, C.D.; Kanjanaboos, P. Novel electrodes for supercapacitor: Conducting polymers, metal oxides, chalcogenides, carbides, nitrides, MXenes, and their composites with graphene. *J. Alloys Compd.* **2021**, *893*, 161998. [[CrossRef](#)]
12. Wang, Q.; Wu, M.; Meng, S.; Zang, X.; Dai, Z.; Si, W.; Huang, W.; Dong, X. Hydrazine Sensor Based on Co<sub>3</sub>O<sub>4</sub>/rGO/Carbon Cloth Electrochemical Electrode. *Adv. Mater. Interfaces* **2016**, *3*, 1500691. [[CrossRef](#)]
13. Cheraghi, S.; Taher, M.A.; Karimi-Maleh, H.; Karimi, F.; Shabani-Nooshabadi, M.; Alizadeh, M.; Al-Othman, A.; Erk, N.; Raman, P.K.Y.; Karaman, C. Novel enzymatic graphene oxide based biosensor for the detection of glutathione in biological body fluids. *Chemosphere* **2021**, *287*, 132187. [[CrossRef](#)] [[PubMed](#)]
14. Shu, R.; Li, X.; Tian, K.; Shi, J. Fabrication of bimetallic metal-organic frameworks derived Fe<sub>3</sub>O<sub>4</sub>/C decorated graphene composites as high-efficiency and broadband microwave absorbers. *Compos. Part B Eng.* **2021**, *228*, 109423. [[CrossRef](#)]
15. Yan, S.; Song, H.; Li, Y.; Yang, J.; Jia, X.; Wang, S.; Yang, X. Integrated reduced graphene oxide/polypyrrole hybrid aerogels for simultaneous photocatalytic decontamination and water evaporation. *Appl. Catal. B Environ.* **2021**, *301*, 120820. [[CrossRef](#)]
16. Qiu, B.; Zhao, X.; Xia, D. In situ synthesis of CoS<sub>2</sub>/RGO nanocomposites with enhanced electrode performance for lithium-ion batteries. *J. Alloys Compd.* **2013**, *579*, 372–376. [[CrossRef](#)]
17. Kong, P.; Zhu, L.; Li, F.; Xu, G. Self-Supporting Electrode Composed of SnSe Nanosheets, Thermally Treated Protein, and Reduced Graphene Oxide with Enhanced Pseudocapacitance for Advanced Sodium-Ion Batteries. *ChemElectroChem* **2019**, *6*, 5642–5650. [[CrossRef](#)]
18. Li, W.; Teng, C.; Sun, Y.; Cai, L.; Xu, J.-L.; Sun, M.; Li, X.; Yang, X.; Xiang, L.; Xie, D.; et al. Sprayed, Scalable, Wearable, and Portable NO<sub>2</sub> Sensor Array Using Fully Flexible AgNPs-All-Carbon Nanostructures. *ACS Appl. Mater. Interfaces* **2018**, *10*, 34485–34493. [[CrossRef](#)]
19. Cui, S.; Pu, H.; Mattson, E.C.; Wen, Z.; Chang, J.; Hou, Y.; Hirschmugl, C.J.; Chen, J. Ultrasensitive Chemical Sensing through Facile Tuning Defects and Functional Groups in Reduced Graphene Oxide. *Anal. Chem.* **2014**, *86*, 7516–7522. [[CrossRef](#)]
20. Yuan, W.; Liu, A.; Huang, L.; Li, C.; Shi, G. High-Performance NO<sub>2</sub> Sensors Based on Chemically Modified Graphene. *Adv. Mater.* **2013**, *25*, 766–771. [[CrossRef](#)]
21. Zhou, Y.; Liu, G.; Zhu, X.; Guo, Y. Ultrasensitive NO<sub>2</sub> gas sensing based on rGO/MoS<sub>2</sub> nanocomposite film at low temperature. *Sens. Actuators B Chem.* **2017**, *251*, 280–290. [[CrossRef](#)]
22. Hung, C.M.; Dat, D.Q.; Van Duy, N.; Van Quang, V.; Van Toan, N.; Van Hieu, N.; Hoa, N.D. Facile synthesis of ultrafine rGO/WO<sub>3</sub> nanowire nanocomposites for highly sensitive toxic NH<sub>3</sub> gas sensors. *Mater. Res. Bull.* **2020**, *125*, 110810. [[CrossRef](#)]

23. Kuchi, C.; Naresh, B.; Reddy, P.S. In Situ TiO<sub>2</sub>-rGO Nanocomposite for Low Concentration NO Gas Sensor. *ECS J. Solid State Sci. Technol.* **2021**, *10*, 37008. [[CrossRef](#)]
24. Li, J.; Jiang, J.; Zhao, D.; Xu, Z.; Liu, M.; Liu, X.; Tong, H.; Qian, D. Novel hierarchical sea urchin-like Prussian blue@palladium core-shell heterostructures supported on nitrogen-doped reduced graphene oxide: Facile synthesis and excellent guanine sensing performance. *Electrochim. Acta* **2020**, *330*, 135196. [[CrossRef](#)]
25. Li, J.; Jiang, J.; Feng, H.; Xu, Z.; Tang, S.; Deng, P.; Qian, D. Facile synthesis of 3D porous nitrogen-doped graphene as an efficient electrocatalyst for adenine sensing. *RSC Adv.* **2016**, *6*, 31565–31573. [[CrossRef](#)]
26. Jung, W.T.; Jeon, J.W.; Jang, H.-S.; Kim, D.Y.; Lee, H.-K.; Kim, B.H. Commercial silk-based electronic textiles for NO<sub>2</sub> sensing. *Sens. Actuators B Chem.* **2020**, *307*, 127596. [[CrossRef](#)]
27. Cho, S.-Y.; Yu, H.; Choi, J.; Kang, H.; Park, S.; Jang, J.-S.; Hong, H.-J.; Kim, I.-D.; Lee, S.-K.; Jeong, H.S.; et al. Continuous Meter-Scale Synthesis of Weavable Tunicate Cellulose/Carbon Nanotube Fibers for High-Performance Wearable Sensors. *ACS Nano* **2019**, *13*, 9332–9341. [[CrossRef](#)]
28. Li, W.; Geng, X.; Guo, Y.; Rong, J.; Gong, Y.; Wu, L.; Zhang, X.; Li, P.; Xu, J.; Cheng, G.; et al. Reduced Graphene Oxide Electrically Contacted Graphene Sensor for Highly Sensitive Nitric Oxide Detection. *ACS Nano* **2011**, *5*, 6955–6961. [[CrossRef](#)]
29. Bai, S.; Shen, X.; Zhu, G.; Yuan, A.; Zhang, J.; Ji, Z.; Qiu, D. The influence of wrinkling in reduced graphene oxide on their adsorption and catalytic properties. *Carbon* **2013**, *60*, 157–168. [[CrossRef](#)]
30. Sharma, N.; Sharma, V.; Sharma, S.K.; Sachdev, K. Gas sensing behaviour of green synthesized reduced graphene oxide (rGO) for H<sub>2</sub> and NO. *Mater. Lett.* **2019**, *236*, 444–447. [[CrossRef](#)]
31. Li, Y.; Huan, K.; Deng, D.; Tang, L.; Wang, J.; Luo, L. Facile Synthesis of ZnMn<sub>2</sub>O<sub>4</sub>@rGO Microspheres for Ultrasensitive Electrochemical Detection of Hydrogen Peroxide from Human Breast Cancer Cells. *ACS Appl. Mater. Interfaces* **2019**, *12*, 3430–3437. [[CrossRef](#)] [[PubMed](#)]
32. Li, C.; Yang, J.; Pachfule, P.; Li, S.; Ye, M.-Y.; Schmidt, J.; Thomas, A. Ultralight covalent organic framework/graphene aerogels with hierarchical porosity. *Nat. Commun.* **2020**, *11*, 4712. [[CrossRef](#)] [[PubMed](#)]
33. Zhu, X.; Guo, Y.; Ren, H.; Gao, C.; Zhou, Y. Enhancing the NO<sub>2</sub> gas sensing properties of rGO/SnO<sub>2</sub> nanocomposite films by using microporous substrates. *Sens. Actuators B Chem.* **2017**, *248*, 560–570. [[CrossRef](#)]
34. Wetchakun, K.; Samerjai, T.; Tamaekong, N.; Liewhiran, C.; Siriwong, C.; Kruefu, V.; Wisitsoraat, A.; Tuantranont, A.; Phanichphant, S. Semiconducting metal oxides as sensors for environmentally hazardous gases. *Sens. Actuators B Chem.* **2011**, *160*, 580–591. [[CrossRef](#)]
35. Liu, W.; Gu, D.; Zhang, J.-W.; Li, X.-G.; Romyantseva, M.N.; Gaskov, A.M. ZnSe/NiO heterostructure-based chemiresistive-type sensors for low-concentration NO<sub>2</sub> detection. *Rare Met.* **2021**, *40*, 1632–1641. [[CrossRef](#)]
36. Deng, S.; Tjoa, V.; Fan, H.M.; Tan, H.R.; Sayle, D.C.; Olivo, M.; Mhaisalkar, S.; Wei, J.; Sow, C.H. Reduced Graphene Oxide Conjugated Cu<sub>2</sub>O Nanowire Mesocrystals for High-Performance NO<sub>2</sub> Gas Sensor. *J. Am. Chem. Soc.* **2012**, *134*, 4905–4917. [[CrossRef](#)]
37. Zanolli, Z.; Leghrib, R.; Felten, A.; Pireaux, J.-J.; Llobet, E.; Charlier, J.-C. Gas Sensing with Au-Decorated Carbon Nanotubes. *ACS Nano* **2011**, *5*, 4592–4599. [[CrossRef](#)]
38. Hoffmann, M.W.G.; Prades, J.D.; Mayrhofer, L.; Hernandez-Ramirez, F.; Järvi, T.T.; Moseler, M.; Waag, A.; Shen, H. Highly Selective SAM-Nanowire Hybrid NO<sub>2</sub> Sensor: Insight into Charge Transfer Dynamics and Alignment of Frontier Molecular Orbitals. *Adv. Funct. Mater.* **2014**, *24*, 595–602. [[CrossRef](#)]
39. Su, Y.; Xie, G.; Tai, H.; Li, S.; Yang, B.; Wang, S.; Zhang, Q.; Du, H.; Zhang, H.; Du, X.; et al. Self-powered room temperature NO<sub>2</sub> detection driven by triboelectric nanogenerator under UV illumination. *Nano Energy* **2018**, *47*, 316–324. [[CrossRef](#)]
40. Zhou, J.; Xue, K.; Liu, Y.; Liang, T.; Zhang, P.; Zhang, X.; Zhang, W.; Dai, Z. Highly sensitive NO<sub>2</sub> response and abnormal P-N sensing transition with ultrathin Mo-doped SnS<sub>2</sub> nanosheets. *Chem. Eng. J.* **2021**, *420*, 127572. [[CrossRef](#)]
41. Sharma, B.; Sharma, A.; Joshi, M.; Myung, J.-H. Sputtered SnO<sub>2</sub>/ZnO Heterostructures for Improved NO<sub>2</sub> Gas Sensing Properties. *Chemosensors* **2020**, *8*, 67. [[CrossRef](#)]
42. Cui, S.; Pu, H.; Wells, S.A.; Wen, Z.; Mao, S.; Chang, J.; Hersam, M.C.; Chen, J. Ultrahigh sensitivity and layer-dependent sensing performance of phosphorene-based gas sensors. *Nat. Commun.* **2015**, *6*, 8632. [[CrossRef](#)] [[PubMed](#)]
43. Kim, J.-O.; Koo, W.-T.; Kim, H.; Park, C.; Lee, T.; Hutomo, C.A.; Choi, S.Q.; Kim, D.S.; Kim, I.-D.; Park, S. Large-area synthesis of nanoscopic catalyst-decorated conductive MOF film using microfluidic-based solution shearing. *Nat. Commun.* **2021**, *12*, 4294. [[CrossRef](#)] [[PubMed](#)]